SH Wave Scattering from Fractures using Boundary Element Method with Linear Slip Boundary Condition

Tianrun Chen , Michael Fehler, Xinding Fang, Xuefeng Shang, Dan Burns, Earth Resource Laboratory, Massachusetts Institute of Technology, Cambridge, Massachusetts 02139

SUMMARY

A boundary element method (BEM) combined with a linear slip boundary condition is proposed to calculate SH wave scattering from fractures. The linear slip boundary condition was proposed by Schoenberg (1980) to model elastic wave propagation through an imperfectly bonded interface, where the traction cross the interface is continuous and displacement is discontinuous. Here, we demonstrate how to simulate SH wave scattering from fractures by applying the BEM and this linear slip boundary. Comparisons between results obtained using our model with those obtained using a computationally expensive finite difference method (FDM) (Coates and Schoenberg, 1995; Krüger et al., 2005) are performed to show the validity and accuracy of our approach. An example of SH wave scattering from three curved, crossing fractures is also given. Although our discussion here is focused on the linear slip boundary condition, our approach can easily be adopted to various slip boundary conditions that specify the displacement discontinuity and traction relations depending on different physical models of fractures.

INTRODUCTION

Underground fracture network characterization and localization are very important for enhanced recovery of oil and gas as well as for guiding the development of geothermal energy reservoirs. This is because the permeability of fractures can be orders of magnitude higher than that of the surrounding matrix. Commonly used techniques to image and characterize these fractures rely heavily on surveys using both surface seismic and vertical seismic profiling (VSP) data (Willis et al., 2006). In order to properly interpret these seismic data for imaging fractures, it is essential to have an accurate and fast method to simulate seismic wave propagation through fractures. This forward modeling problem has been extensively discussed in various literature using different physical models of fractures combined with analytical and numerical techniques including BEM (Kelner et al., 1999; Pointer et al., 1998; Iturrarán-Viveros et al., 2005, 2008; Gu et al., 1997), FDM (Fehler and Aki, 1978; Coates and Schoenberg, 1995; Krüger et al., 2005; Groenenboom and Falk, 2000; Vlastos et al., 2003; Slawinski and Krebes, 2002; Zhang, 2005; Zhang and Gao, 2009), Finite Element Method (FEM) (Nakagawa et al., 2003) and analytical methods(Liu et al., 1997; Sánchez-Sesma and Iturrarán-Viveros, 2001). Compared to the FDM, FEM and analytical methods, BEM is potentially more flexible and accurate in handling complicated fracture boundary shapes and conditions. It is more computationally efficient since it needs to compute one less space dimension than FDM and FEM except for some scenarios with special geometries of fracture sets (Nakagawa et al., 2003). The major drawback of BEM is that the computational cost can be very high for 3D fractures or large 2D fracture networks. This issue may potentially be solved by applying fast multi-pole method(FMM) (Greengard and Gropp, 1990).

In this paper, we apply BEM and the linear slip boundary condition to simulate the scattering of SH waves from 2D fractures. The use of the linear slip boundary condition makes our model appropriate for the modeling of fractures in real rock. Another advantage of our method is that it is not restricted to the linear slip boundary condition and can also flexibly implement other slip boundary conditions that specify the relation between the displacement discontinuities and traction across a fracture surface, as described by various authors (Fehler, 1982; Liu et al., 1995; Hudson et al., 1996; Liu et al., 2000; Bakuh and Molotkov, 1997; Nakagawa and Schoenberg, 2007).

BEM MODELING OF SCATTERING FROM FRACTURES

In this section, we will first show mathematical derivations for applying BEM to calculate the scattering from a single 2D fracture with the linear slip condition and then briefly discuss the calculation of scattering from multiple 2D fractures.

Scattering from a 2D fracture

The scattered displacement (Aki and Richards, 1980) from a fracture in the free space is expressed as

$$u_i^{\mathrm{sca}}(x) = \int_s [u_k(\xi)] C_{kjqp}(\xi) \frac{\partial G_i^p(x,\xi)}{\partial \xi_q} n_j(\xi) \mathrm{d}\xi \qquad (1)$$

where ξ is a point on the 2D fracture surface s, as shown in Figure 1; $C_{kjqp}(\xi)$ is the elastic tensor; $G_i^p(x,\xi)$ is the i^{th} displacement component of the Green's function at point x due to a unit force in the p^{th} direction at point ξ on the fracture surface; n_j is the j^{th} component of the normal vector n at the fracture surface S; $[u_k(\xi)]$ is the k^{th} component of the displacement discontinuity

$$[u_k(\xi)] = u_k^+(\xi) - u_k^-(\xi), \qquad (2)$$

where $u_k^+(\xi)$ and $u_k^-(\xi)$ is the total displacement on the upper and lower surface of the fracture, respectively.

The total displacement field $u_k(\xi)$ is the sum of the incident and scattered displacement. In this paper, the displacement discontinuity is determined from the linear slip condition (Schoenberg, 1980), which assumes that the displacement discontinuity is linearly proportional to the traction on the fracture surface, and the traction is continuous across the fracture. For the SH wave, we have

$$\begin{aligned}[u_2(\xi)] &= Z_t(\xi)\ \sigma_{21}(\xi) n_1(\xi) + \sigma_{23}(\xi) n_3(\xi) \\ &= Z_t(\xi)\ \mu \frac{\partial u_2(\xi)}{\partial \xi_1} n_1(\xi) + \mu \frac{\partial u_2(\xi)}{\partial \xi_3} n_3(\xi) \qquad (3)\end{aligned}$$

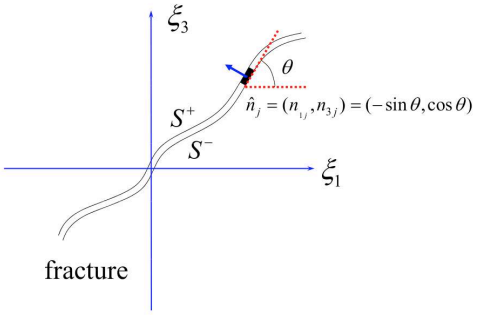

Figure 1: Geometry of a 2D fracture

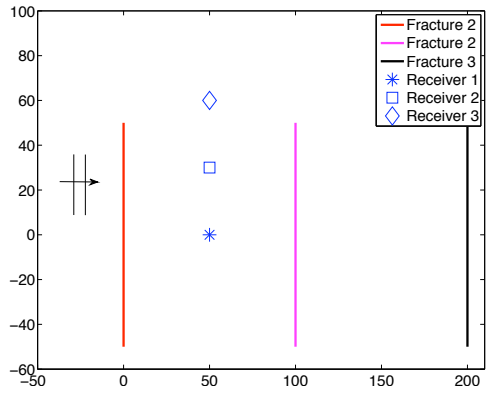

Figure 2: Geometry of three parallel fractures and receivers. A plane wave is normal incident on the fracture from the left

where Z_t is the tangential compliance defined by Schoenberg (1980). Inserting Equation 3 into Equation 1, we can express the scattered field as

$$u_2^{\text{sca}}(x) = \int_s Z_t(\xi)\mu^2 \left[\frac{\partial u_2(\xi)}{\partial \xi_1} n_1(\xi) + \frac{\partial u_2(\xi)}{\partial \xi_3} n_3(\xi) \right] \left[\frac{\partial G(x,\xi)}{\partial \xi_1} n_1(\xi) + \frac{\partial G(x,\xi)}{\partial \xi_3} n_3(\xi) \right] \mathrm{d}\xi. \quad (4)$$

where $G(x,\xi) = G_2^2(x,\xi)$. The displacement at any x is the sum of the incident and scattered displacement

$$u_2(x) = u_2^{\text{inc}}(x) + u_2^{\text{sca}}(x). \quad (5)$$

For a point on the fracture surface $x(x_1, x_3) \quad s$, it should satisfy Equation 5

$$u_2(x) = u_2^i(x) + \int_s Z_t(\xi)\mu^2 \left[\frac{\partial u_2(\xi)}{\partial \xi_1} n_1(\xi) + \frac{\partial u_2(\xi)}{\partial \xi_3} n_3(\xi) \right] \left[\frac{\partial G(x,\xi)}{\partial \xi_1} n_1(\xi) + \frac{\partial G(x,\xi)}{\partial \xi_3} n_3(\xi) \right] \mathrm{d}\xi, \quad (6)$$

where $\int_s$ donates the hyper-singular integral equation or a Cauchy's principal value. We take derivatives of Equation 6 over x_1 and x_3, respectively

$$\frac{\partial u_2(x)}{\partial x_1} = \frac{\partial u_2^i(x)}{\partial x_1} + \int_s Z_t(\xi)\mu^2 \left[\frac{\partial u_2(\xi)}{\partial \xi_1} n_1(\xi) + \frac{\partial u_2(\xi)}{\partial \xi_3} n_3(\xi) \right] \left[\frac{\partial^2 G(x,\xi)}{\partial \xi_1 \partial x_1} n_1(\xi) + \frac{\partial^2 G(x,\xi)}{\partial \xi_3 \partial x_1} n_3(\xi) \right] \mathrm{d}\xi, \quad (7)$$

and

$$\frac{\partial u_2(x)}{\partial x_3} = \frac{\partial u_2^i(x)}{\partial x_3} + \int_s Z_t(\xi)\mu^2 \left[\frac{\partial u_2(\xi)}{\partial \xi_1} n_1(\xi) + \frac{\partial u_2(\xi)}{\partial \xi_3} n_3(\xi) \right] \left[\frac{\partial^2 G(x,\xi)}{\partial \xi_1 \partial x_3} n_1(\xi) + \frac{\partial^2 G(x,\xi)}{\partial \xi_3 \partial x_3} n_3(\xi) \right] \mathrm{d}\xi, \quad (8)$$

by applying a theorem proved by Martin and Rizzo (1989). We now turn the displacement boundary integral equation (1) into two traction-related boundary integral equations (7 and 8).

Solving these two equations provides values of the displacement derivitive $\frac{\partial u_2(x)}{\partial x_1}$ and $\frac{\partial u_2(x)}{\partial x_3}$ across the fracture. By inserting these two derivitives into Equation 4, the displacement field scattered from the 2D fracture can be finally calculated.

Scattering from multiple fractures

In order to calculate the scattering from multiple fractures, we need to calculate the scattered field on fracture i due to the displacement discontinuity on fracture j

$$u_2^{\text{sca}}(x_i) = \int_s Z_t(\xi_j)\mu^2 \left[\frac{\partial u_2(\xi_j)}{\partial \xi_{1j}} n_1(\xi_j) + \frac{\partial u_2(\xi_j)}{\partial \xi_{3j}} n_3(\xi_j) \right] \left[\frac{\partial G_2^2(x_i,\xi_j)}{\partial \xi_{1j}} n_1(\xi_j) + \frac{\partial G_2^2(x_i,\xi_j)}{\partial \xi_{3j}} n_3(\xi_j) \right] \mathrm{d}\xi_j \quad . \quad (9)$$

Different from equation 4, Equation 9 does not need to handle the singularity issue since x_i and ξ_j are elements belonging to different fractures. We need to solve four unknowns $\frac{\partial u_2(x_i)}{\partial x_{1i}}$, $\frac{\partial u_2(x_i)}{\partial x_{3i}}$, $\frac{\partial u_2(x_j)}{\partial x_{1j}}$, and $\frac{\partial u_2(x_j)}{\partial x_{3j}}$ simultaneously to include the coupling between different fractures, which requires a larger matrix inversion compared to a single fracture scenario. The computation cost dramatically increases as the number of fractures increases, which makes this method impractical for a large and complex fracture networks. One way to avoid the large matrix inversion is to apply an iterative method that calculates and sums enough orders of multiple scattering (Born series) until the traction across the fracture surface is converged. This method has been discussed in much more details in Kelner et al. (1999). The iterative method could reduce the computational cost since it only needs to perform the inversion of the coefficient matrix for each individual fracture. The iterative method, however, may not always converge especially when the scattering from fractures is very strong compared to the incident field. In the future, we may consider developing a hybrid method combining matrix inversion method and the iterative method to calculate the multiple scattering from a fracture network.

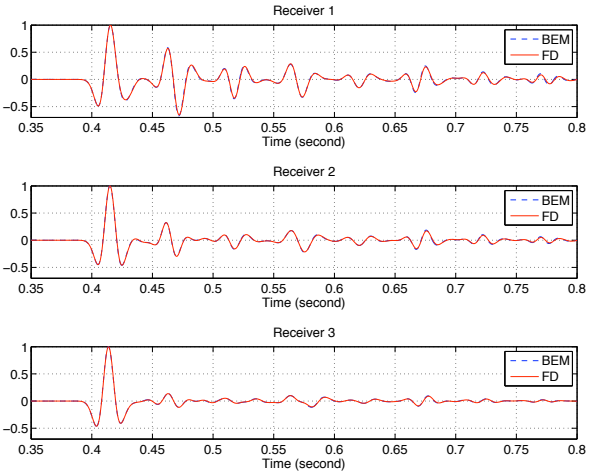

Figure 3: Comparison of received time traces between BEM and FD.

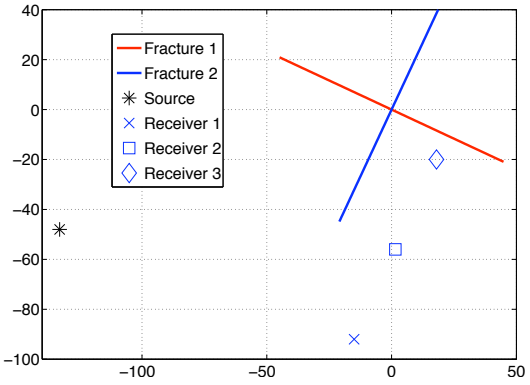

Figure 4: Geometry of two orthogonal fractures, source and receivers.

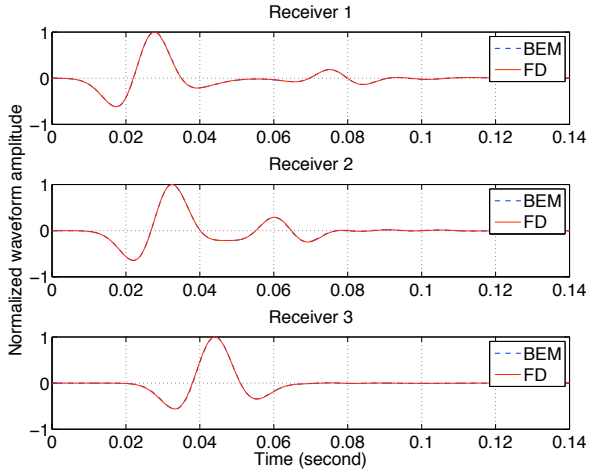

Figure 5: Comparison of received time traces between BEM and FD. The geometry of source, receivers and fractures are rotated in FD simulation correspondingly to make fractures coincide with grids.

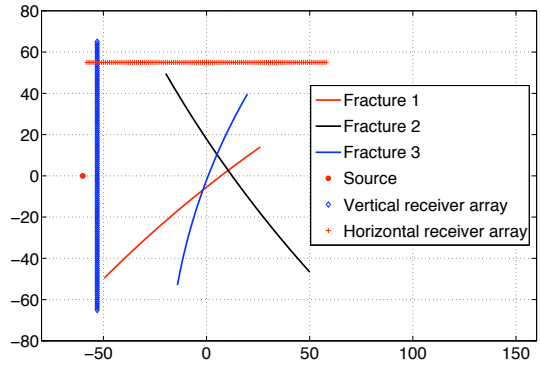

Figure 6: Geometry of source, horizontal and vertical receiver arrays and three curved and crossed fractures.

VERIFICATION AND ILLUSTRATIVE NUMERICAL EXAMPLE

In this section, we first provide two examples where we compare results of using our BEM method for simulating fracture scattering with these obtained by using the FDM (Coates and Schoenberg, 1995). We then show an example of the scattering of SH waves from three curved fractures that cross over each other. The FDM that we use is fourth order in space and second order in time. We used a grid interval of 1 m. For the BEM method, we calculate the complete scattered displacement field by simultaneously inverting the coupled equations (7, 8 and 9).

For all examples, fractures are taken to be embedded in a homogeneous medium with shear velocity 2000 m/s and density 2200 kg/m^3. The tangential compliance of the fractures Z_t is $10^{-9} m/Pa$. A plane wave with a 40 Hz Ricker time-history is normally incident on the fractures.

In example 1, the lengths of the three fractures are 100 m and the wavelength at 40 Hz is 50 m, as shown in Figure 2. Figure 3 shows the comparison of the waveforms simulated using BEM and FDM at three receivers. We find an excellent match between these two methods.

In example 2, we show the comparison of traces from two orthogonal fractures whose geometry is shown in Figure 4. The elevation angles of the fractures are 65 and 155 degree respectively. For the FDM, we rotated the fractures to make them coincident with grids and also rotated the source and receiver locations to maintain the same geometry. The comparison between two methods is very good, as shown in Figure 5.

Finally, we show the scattered SH displacement field (Incident field is purposely removed) from more geologically complicated fractures that are curved and crossing over each other, as shown in Figure 6. The scattered fields received on a vertical array is shown in Figure 7(a), which shows several distinguishable events due to the primary scattering from three fractures and multiple scattering between fractures. Figure 7(b) shows the scattered fields received on a horizontal array, which also contains complicated scattered arrivals from fractures.

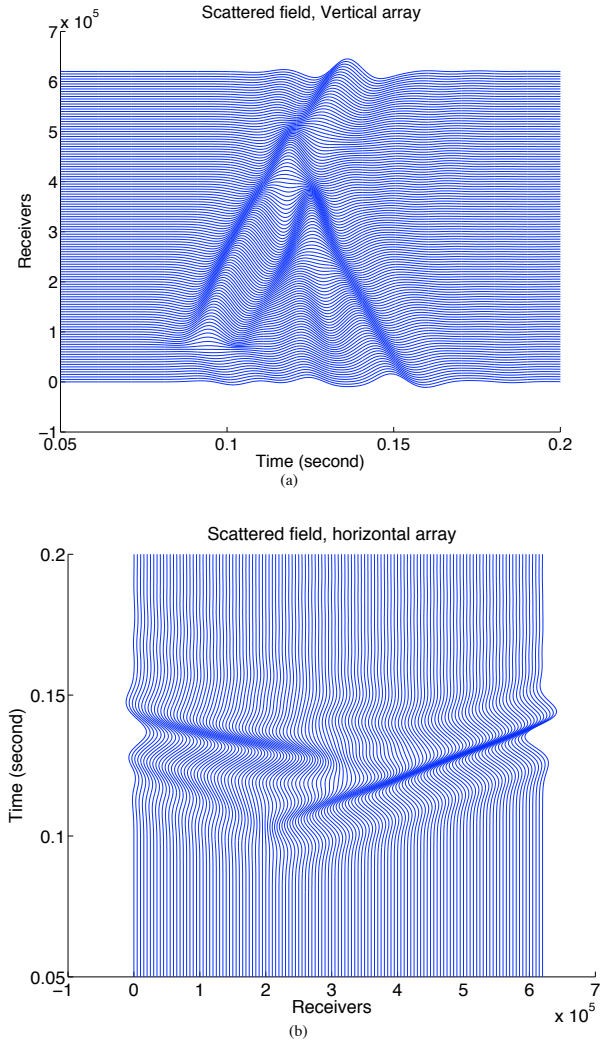

Figure 7: (a) Received time traces on the vertical array (b) Received time traces on the horizontal array.

CONCLUSION

In this paper, we propose a method to use BEM with a linear slip boundary condition to calculate SH wave scattering from 2D fractures that are characterized by the linear slip boundary condition, and show the validity and accuracy of our method by comparing with FDM. This method can also easily adopt other slip boundary conditions and calculate seismic scattering from fracture networks with complex geometries. Because of computational efficiency and accuracy of BEM, our method can potentially be used to perform Monte-Carlo simulations to characterize the statistics of scattering signal from underground fractures.

ACKNOWLEDGMENTS

This work is funded by the Eni Multiscale Reservoir Science Project within the Eni-MIT Energy Initiative Founding Member Program.